materials

MDPI

Article

Organic–Inorganic Stabilization of Expansive Tuff Spoil for Cement-Stabilized Pavement Bases: Laboratory Characterization and Field Validation

Long Ma [1], Shen Zuo [1,*], Jin Li [1,*], Henggen Zhang [1,2] and Junwei Bi [1,3]

[1] Shandong Key Laboratory of Technologies and Systems for Intelligent Construction Equipment, Shandong Jiaotong University, Jinan 250357, China
[2] Shandong Engineering Research Center of Marine Exploration and Conservation, Ocean University of China, Qingdao 266100, China
[3] Department of Geotechnical Engineering & Key Laboratory of Geotechnical and Underground Engineering of Ministry of Education, Tongji University, Shanghai 200092, China
* Correspondence: zuoshen2006@163.com (S.Z.); 204026@sdjtu.edu.cn (J.L.)

Abstract

Moisture-sensitive expansive tuff spoil is difficult to utilize directly in cement-stabilized pavement bases because of its susceptibility to water-induced deformation and associated mechanical and volumetric instability. This study developed an organic–inorganic stabilization system based on sodium silicate nonahydrate ($Na_2SiO_3 \cdot 9H_2O$) and cationic polyacrylamide (CPAM) and established a staged screening–validation framework combining swelling, mechanical, shrinkage, microstructural, and field evaluations. Within the tested range, the formulation containing 5.0% $Na_2SiO_3 \cdot 9H_2O$ and 0.5% CPAM reduced the free swelling rate from 5.0% to 0.517%, corresponding to an 89.7% reduction. At 28 d, the mean unconfined compressive strength (UCS), splitting tensile strength (STS), and compressive resilient modulus were 15.61%, 27.0%, and 7.9% higher, respectively, than those of the cement-stabilized control. After Holm adjustment, STS showed statistically significant improvements at all tested curing ages, whereas UCS differed significantly only at 14 d, and compressive resilient modulus showed no statistically significant differences. The 90-d cumulative drying shrinkage strain (CDSS) decreased by 37.8%, while the thermal shrinkage coefficient (TSC) remained lower than that of the control over the tested temperature range. XRD and SEM–EDS analyses indicated that the dominant crystalline phases remained essentially unchanged, while qualitative SEM observations revealed a more compact interparticle morphology and fewer visible macropores in the modified material. These observations suggest possible contributions from improved interparticle bonding and interfacial regulation to the overall performance improvement. A 267-m full-scale expressway test section constructed using double-layer continuous paving achieved upper- and lower-layer compaction degrees of 98.6% and 98.4%, respectively, an average 7-d field UCS of 5.16 MPa, and a surface-evenness acceptance rate above 96%. These results support the feasibility of utilizing moisture-sensitive tuff spoil in cement-stabilized pavement bases under the tested laboratory and field conditions, providing evidence of its constructability and satisfactory early-age performance.

Keywords: expansive tuff spoil; cement-stabilized pavement base; organic–inorganic stabilization; swelling; shrinkage; field validation

Check for updates

Academic Editor: Zhidong Zhang

Received: 24 October 2026
Revised: 4 November 2026
Accepted: 8 November 2026
Published: 13 November 2026

Copyright: © 2026 by the authors. Licensee MDPI, Basel, Switzerland. This article is an open access article distributed under the terms and conditions of the Creative Commons Attribution (CC BY) license.

1. Introduction

The continued development of transportation infrastructure has increased the demand for natural aggregates, raising concerns about resource consumption and the environmental impacts of aggregate extraction [1–3]. Utilizing excavation spoil and alternative geomaterials can help reduce reliance on virgin aggregates [4–6]. Previous studies have demonstrated the potential of tunnel excavation spoil and volcanic aggregates for construction and pavement applications [7–9]. However, the engineering behavior of tuff depends strongly on its mineral composition, pore structure, and degree of weathering. Moisture-sensitive tuffs may undergo structural softening and volumetric deformation upon water exposure [10–12]. Increasing moisture content can also reduce the resilient response and increase accumulated deformation of crushed tuff aggregates under cyclic loading [13]. Accordingly, controlling moisture-induced deformation while maintaining adequate load-bearing capacity and cracking resistance remains a key challenge when using expansive tuff spoil in cement-stabilized semi-rigid pavement bases.

Chemical stabilization is widely used to improve expansive and moisture-sensitive geomaterials through mechanisms such as cation exchange, hydration, cementation, and pozzolanic reactions [14,15]. Chloride-based treatments suppress clay swelling through ion exchange [16,17], whereas silicate-based and other inorganic stabilizers enhance interparticle bonding through cementitious reactions [18–21]. Combining recycled mineral additives with natural fibers has also been reported to improve the swelling resistance, strength, and durability of expansive soils [22]. However, previous studies have primarily focused on fine-grained expansive soils or artificially prepared soil systems. The applicability of these stabilization approaches to cement-stabilized tuff, comprising a coarse aggregate skeleton, fine tuff particles, and a cementitious matrix, remains insufficiently understood.

Organic polymers offer an alternative stabilization approach by regulating particle surfaces, interparticle interactions, and water–mineral interactions [23]. Cationic polyacrylamide (CPAM) can suppress the swelling of montmorillonite and expansive soils while improving their water stability and mechanical properties [24,25]. Cationic surfactants, such as hexadecyltrimethylammonium bromide (HTAB), can also modify clay-mineral surfaces and interlayer characteristics [26]. Unlike inorganic stabilizers, organic polymers primarily regulate interfacial interactions rather than forming a rigid cementitious skeleton. Combining inorganic cementation with organic interfacial modification may therefore provide complementary benefits by controlling moisture-induced deformation while maintaining the mechanical integrity required for pavement bases.

Previous studies have examined tunnel excavation spoil in cement-stabilized pavement bases [7], multi-source stabilizer proportioning [27], and organic–inorganic modification of steel-slag cement-stabilized macadam [28]. Related research has also addressed expansive subgrade stabilization [29], soil–aggregate–cement mixtures [30], and the thermal response of cement-stabilized aggregates [31]. However, the simultaneous control of moisture-induced swelling and maintenance of mechanical and volumetric stability in cement-stabilized expansive tuff spoil remain insufficiently investigated. Unlike the materials examined in [7,28], moisture-sensitive tuff requires a combined evaluation of modifier selection, mechanical and shrinkage performance, and microstructural characteristics. These issues warrant systematic investigation before its broader application in pavement bases.

Construction procedures play an important role in the structural integrity of cement-stabilized pavement bases. Double-layer continuous paving has been shown to improve structural densification and interlayer bonding [32–34]. However, its applicability to organic–inorganic modified tuff mixtures remains insufficiently investigated and requires field validation [35,36].

It was hypothesized that combining inorganic stabilization with organic interfacial modification could provide complementary benefits for expansive tuff spoil. Specifically, inorganic modifiers were expected to improve particle bonding and structural stability, while organic polymers could regulate interfacial interactions and contribute to swelling suppression. Their combination was therefore expected to improve volumetric stability while maintaining or enhancing mechanical performance. To examine this hypothesis, the present study investigated the organic–inorganic stabilization of moisture-sensitive expansive tuff spoil excavated from the Mingcun–Dongjiakou Expressway. Different inorganic and organic modifiers and their combinations were screened using the free swelling rate as the primary criterion. The selected formulation was subsequently evaluated in terms of mechanical properties, drying and thermal shrinkage, and microstructural characteristics using XRD and SEM–EDS. Finally, a 267-m full-scale field trial employing double-layer continuous paving was conducted to assess constructability, construction quality, and early-age performance.

2. Materials and Methods

2.1. Materials

Tuff spoil was obtained from tunnel excavation along the Mingcun–Dongjiakou Expressway and separated into four aggregate fractions (20–30, 10–20, 5–10, and 0–5 mm) after crushing and sieving. XRF analysis showed that SiO_2 (58.79 wt.%) and Al_2O_3 (17.82 wt.%) were the predominant oxides, accounting for 76.61 wt.% in total (Table 1). XRD identified quartz and albite as the dominant crystalline phases (Figure 1), while SEM revealed rough, irregular particle surfaces, local pores, and adhering lamellar fines (Figure 2). These features indicate a heterogeneous microstructure consistent with the moisture sensitivity reported for weathered tuff [10–12].

Table 1. Chemical composition of raw tuff spoil determined by XRF (wt.%).

Material	SiO_2	Al_2O_3	Fe_2O_3	CaO	MgO	Na_2O	K_2O	TiO_2	LOI
Tuff spoil	58.79	17.82	3.44	2.99	2.12	4.46	2.32	0.83	7.23

Note: LOI denotes loss on ignition.

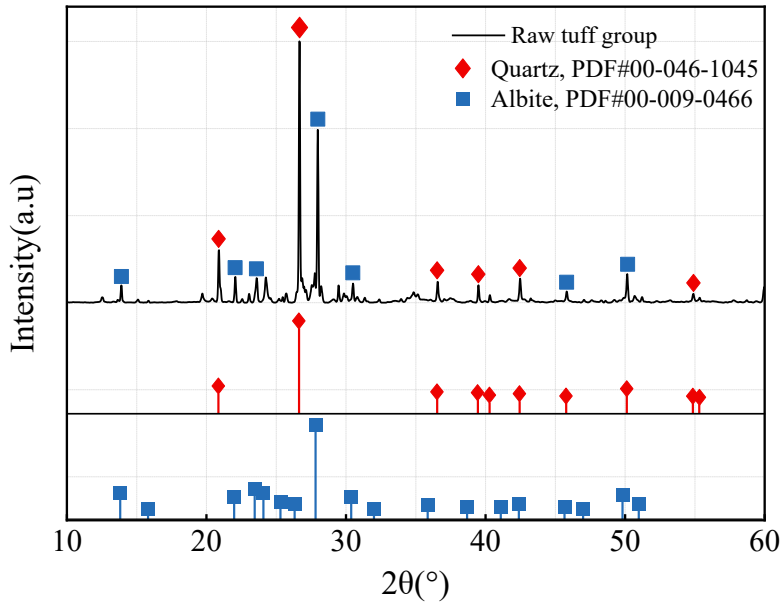

Figure 1. XRD pattern of raw tuff aggregate.

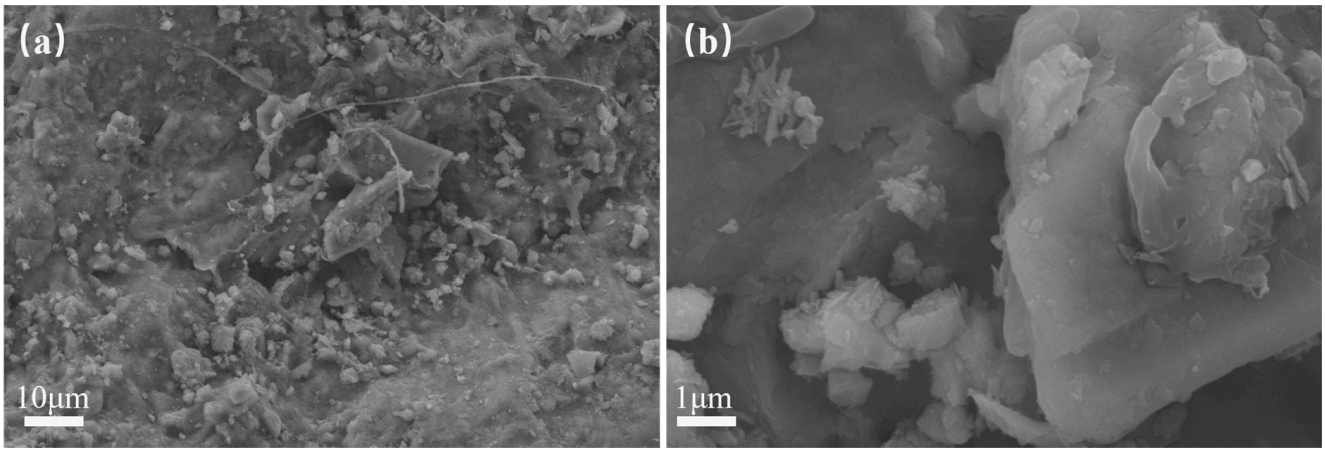

Figure 2. SEM micrographs of raw tuff aggregate: (**a**) 1000×; (**b**) 10,000×.

The physical properties of the aggregate fractions are summarized in Table 2. Apparent density ranged from 2.706 to 2.723 g/cm^3, and bulk specific gravity from 2.668 to 2.690. The flat and elongated particle content of the coarse fractions was at most 7.1%, meeting the requirements for expressway base aggregates in JTG/T F20-2015 [37]. Water absorption increased as particle size decreased, from 0.36% for the 20–30 mm fraction to 1.04% for the 0–5 mm fraction, indicating greater water absorption by finer particles.

Table 2. Basic physical properties of tuff aggregates with different particle size fractions.

Particle Size (mm)	Apparent Density (g/cm^3)	Bulk Specific Gravity	Flat & Elongated Particles (%)	Water Absorption (%)
20–30	2.717	2.688	5.8	0.36
10–20	2.712	2.675	6.2	0.47
5–10	2.706	2.690	7.1	0.63
0–5	2.723	2.668	–	1.04

P·O 42.5 ordinary Portland cement (OPC) was used as the binder, with its principal physical and mechanical properties presented in Table 3. Three inorganic modifiers—aluminum chloride hexahydrate ($AlCl_3 \cdot 6H_2O$), calcium chloride ($CaCl_2$), and sodium silicate nonahydrate ($Na_2SiO_3 \cdot 9H_2O$)—and two organic modifiers, CPAM and HTAB, were selected based on stabilization approaches reported for expansive and moisture-sensitive geomaterials [16–26]. All modifier dosages were expressed as percentages of the dry aggregate mass. Before mixing, the modifiers were dissolved in the mixing water, which met the applicable highway engineering requirements.

Table 3. Technical properties of P·O 42.5 OPC.

Property	Curing Age	Test Result	Standard Requirement
Fineness (%)	–	6.0	≥5.0
Density (g/cm^3)	–	3.06	3.0–3.15
Initial setting time (min)	–	372	≥80
Final setting time (min)	–	482	360–600
Soundness (mm)	–	1	≤5

Table 3. *Cont.*

Property	Curing Age	Test Result	Standard Requirement
Flexural strength (MPa)	3 d	4.9	≥4.0
	28 d	7.9	≥6.5
Compressive strength (MPa)	3 d	26.4	≥17.0
	28 d	50.0	≥42.5

2.2. Mix Design and Specimen Fabrication

Four aggregate gradations were designed within the envelope specified in JTG/T F20-2015 [37] (Figure 3) and evaluated through compaction and 7-d UCS tests. Based on their compaction characteristics and strength performance, gradation 3 was selected as the reference gradation, with mass proportions of 20%, 36%, 15%, and 29% for the 20–30, 10–20, 5–10, and 0–5 mm fractions, respectively.

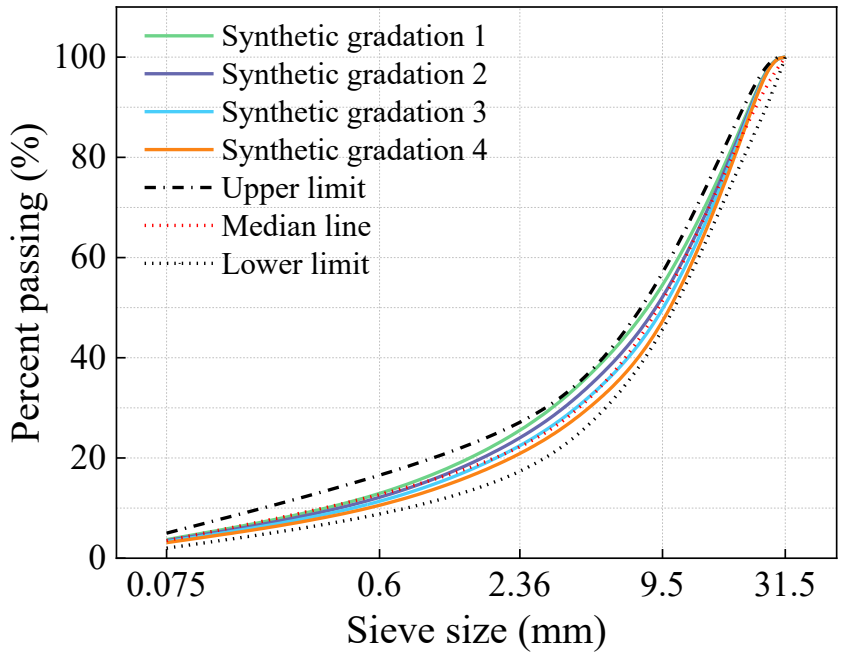

Figure 3. Gradation curves of four synthetic aggregates and specification limits.

Cement contents of 4.0%, 4.5%, and 5.0% (by dry aggregate mass) were evaluated using the reference gradation. A cement content of 4.5% was selected based on strength performance and cement consumption. OMC and MDD were determined for the cement-stabilized control mixture using five moisture contents, yielding values of 7.6% and 2.192 g/cm^3, respectively. These parameters were not independently determined for the composite-modified mixture.

The incorporation of sodium silicate and CPAM may alter water demand and particle interactions, potentially affecting the compaction characteristics of the mixture. However, their effects on OMC and MDD were not independently evaluated in the present study and remain to be quantified.

A staged modifier-screening program was conducted using single modifiers, same-category binary combinations, and organic–inorganic combinations. Free swelling rate was used as the primary screening criterion. Based on the results, a composite formulation containing 5.0% $Na_2SiO_3 \cdot 9H_2O$ and 0.5% CPAM (both by dry aggregate mass) was selected

for subsequent evaluation. Mechanical performance was not used to rank the candidate formulations; the selected mixture was subsequently assessed through mechanical, shrinkage, and microstructural tests. At the selected proportions, each tonne of dry aggregate required approximately 50 kg of $Na_2SiO_3 \cdot 9H_2O$, 5 kg of CPAM, and 45 kg of cement. These quantities provide a basis for estimating material consumption, although no quantitative cost comparison was conducted. Cement-stabilized tuff without additional modifiers served as the control for mechanical and shrinkage tests. For free swelling tests, tuff powder passing a 0.5 mm sieve was used. Untreated powder served as the baseline control, while modified powders were prepared with the prescribed modifier dosages. This consistent particle-size range enabled comparison of the swelling-suppression effects of different modifier systems. The powder specimens were prepared separately from the full-graded aggregate specimens used for mechanical and shrinkage tests, allowing the swelling response of the fine tuff fraction to be evaluated independently of the coarse aggregate skeleton.

Specimens were prepared by static compaction using a hydraulic press. Cylindrical specimens (150 mm in diameter and 150 mm in height) were used for mechanical tests, and prismatic specimens (100 × 100 × 400 mm) for shrinkage tests. After molding, the specimens were held for 24 h before demolding and cured at 20 ± 2 °C and a relative humidity of at least 97%. These curing conditions applied to the mechanical and shrinkage specimens; powdered specimens for free swelling tests were conditioned according to the adopted test procedure. Mechanical tests were performed at curing ages of 7, 14, 28, and 90 d. Before testing, all mechanical specimens underwent 24 h of water immersion; thus, the 7-d specimens were moist-cured for 6 d before immersion. Six replicate specimens were prepared for each mechanical test condition. Results are reported as the mean ± standard deviation (SD), calculated from the six replicates.

2.3. Test Methods

Macroscopic tests included free swelling, mechanical testing, and shrinkage measurements. Free swelling tests were conducted according to GB/T 50123-2019 [38] using tuff powder passing a 0.5 mm sieve. The graduated-cylinder method was used to measure the swelling response of the powder, with free swelling rate serving as the primary criterion for comparing modifier systems. This test characterized the fine tuff fraction rather than the volumetric expansion of the full-graded cement-stabilized mixture. The contour plots presented in this study were generated in OriginPro 2024 using the XYZ gridding to matrix function, Random (Renka–Cline) interpolation, and a 30 × 30 grid. The measured swelling rates at the tested dosage combinations were used as input data, with the two modifier dosages as independent variables. Interpolation was used only to visualize continuous dosage–response relationships; grid values were not treated as additional measurements. Thus, minimum values derived from the contour plots are interpolation-based estimates unless they coincide with an original experimental data point. UCS, splitting tensile strength (STS), and compressive resilient modulus were measured using methods T0805, T0806, and T0807, respectively, in JTG 3441-2024 [39]. Drying and thermal shrinkage were measured using methods T0854 and T0855, respectively, to characterize moisture- and temperature-induced volumetric deformation. Free swelling tests were used to screen modifier systems, whereas mechanical and shrinkage tests compared the selected composite-modified mixture with the cement-stabilized control.

For quantitative analysis, the mean and standard deviation (SD) were calculated from six replicate specimens for each test condition. Error bars in the figures represent ±1 SD of the corresponding experimental measurements. Differences between the control and modified groups at each curing age were evaluated using Welch's independent-samples

t-test. Holm adjustment was applied to account for multiple comparisons across the four curing ages for each mechanical parameter, with statistical significance set at $p < 0.05$.

Microstructural characterization was performed using XRD and SEM–EDS on raw tuff, together with control and composite-modified specimens cured for 28 d. XRD was used to characterize the major crystalline phases and hydration-related phase changes. SEM was used to examine particle morphology, pore characteristics, and interfacial features, while EDS was used to analyze the elemental composition and distribution within selected regions. The microstructural observations were used to interpret the structural features associated with the macroscopic performance changes and to provide supporting evidence for the proposed stabilization mechanisms. Before SEM–EDS analysis, the specimens were sputter-coated with gold to improve electrical conductivity. Accordingly, the detected Au signal originated from the conductive coating rather than the specimen composition and was excluded from the reported elemental compositions. The weight percentages of the remaining elements were retained without further normalization. One EDS elemental mapping field of view was analyzed for each sample group, and the results were used for semi-quantitative comparison of local elemental compositions.

3. Results and Analysis

3.1. Swelling Inhibition Performance

The free swelling rate was adopted as the primary criterion for screening different modifier systems. Untreated tuff powder exhibited a free swelling rate of 5.0%, which served as the baseline for evaluating swelling suppression. Accordingly, the inorganic, organic, and combined modifier systems were compared to identify a suitable composite formulation for subsequent performance evaluation. In this study, "expansive tuff spoil" refers to engineering material exhibiting moisture-induced swelling, rather than indicating the identification of a specific expansive mineral phase. The measured free swelling rate characterizes the swelling response of powdered tuff specimens (particle size < 0.5 mm) used for modifier screening and does not directly represent the volumetric expansion of the full-graded cement-stabilized aggregate mixture.

3.1.1. Single-Modifier Screening

Figure 4 presents the effects of individual inorganic and organic modifiers on the free swelling rate, highlighting their distinct dosage–response characteristics.

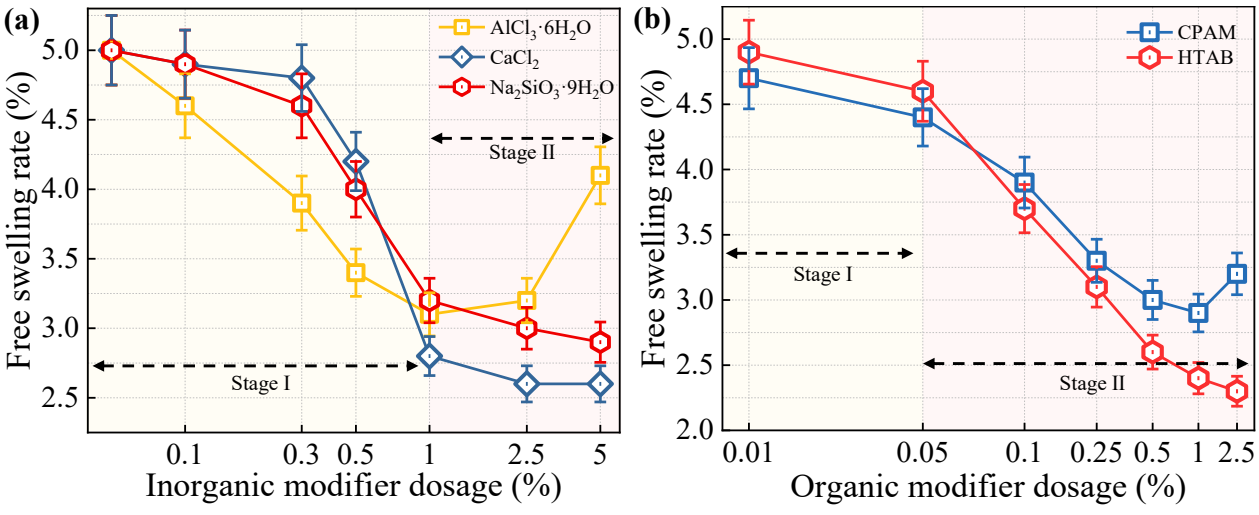

Figure 4. Effect of single-component inorganic and organic modifier dosage on the free swelling rate of tuff. (**a**) Inorganic modifiers; (**b**) organic modifiers. Error bars represent ±1 SD.

The inorganic modifiers exhibited a two-stage dosage response (Figure 4a). In Stage I (0–1.0%), the free swelling rate decreased with increasing dosage for all three modifiers, whereas their responses diverged above 1.0%. $AlCl_3 \cdot 6H_2O$ decreased to approximately 3.1% at 1.0% dosage but subsequently increased to 4.1%. $CaCl_2$ continued to decrease and stabilized at approximately 2.6% over the 2.5–5.0% dosage range. In contrast, $Na_2SiO_3 \cdot 9H_2O$ decreased continuously, reaching 2.9% at 5.0%, corresponding to a 42.0% reduction relative to the control. This trend is consistent with previous studies on silicate-containing stabilization systems [18–21]. Considering its continuous dosage response and avoidance of chloride introduction, $Na_2SiO_3 \cdot 9H_2O$ was selected for subsequent composite screening.

The organic modifiers also exhibited stage-dependent dosage responses (Figure 4b). In Stage I (0.01–0.05%), both CPAM and HTAB produced limited reductions in free swelling rate, whereas stronger suppression occurred above 0.05%. For CPAM, the rate decreased to 3.0% at 0.5% dosage, changed marginally to 2.9% at 1.0%, and increased to 3.2% at 2.5%, indicating limited additional benefit beyond 0.5%. This response is consistent with previous findings on polyacrylamide-based treatments of expansive materials [24,25]. By contrast, HTAB continuously reduced the swelling rate to 2.3% at 2.5%, but required a substantially higher dosage than CPAM.

Based on their swelling-suppression effectiveness and dosage requirements, $Na_2SiO_3 \cdot 9H_2O$ and CPAM were selected as the inorganic and organic components, respectively, for subsequent composite screening.

3.1.2. Same-Category Binary Combinations

Figure 5 presents the response-surface contours of same-category binary combinations, showing that their swelling-suppression effectiveness depended on the modifier combination and did not consistently exceed that of individual modifiers.

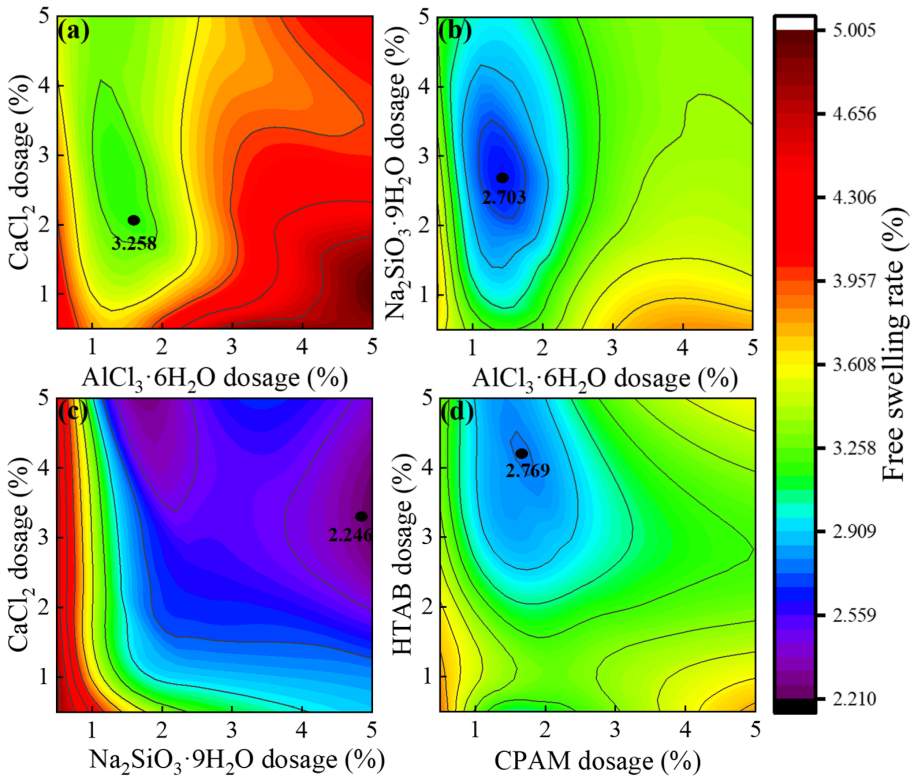

Figure 5. Response-surface contour plots of free swelling rate for same-category binary modifier combinations. (**a**–**c**) Inorganic binary combinations; (**d**) organic binary combination.

Among the inorganic binary systems, $AlCl_3 \cdot 6H_2O$–$CaCl_2$ (Figure 5a) had an interpolated minimum free swelling rate of approximately 3.258%, offering no improvement over the individual modifiers. $Na_2SiO_3 \cdot 9H_2O$–$AlCl_3 \cdot 6H_2O$ (Figure 5b) achieved an interpolated minimum of approximately 2.703%, representing a modest improvement. $Na_2SiO_3 \cdot 9H_2O$–$CaCl_2$ (Figure 5c) performed best, with an interpolated minimum of approximately 2.246%, lower than those obtained with either individual modifier. Similar composition-dependent effects have been reported for multicomponent stabilization systems [20,21,27]. Despite its favorable swelling suppression, the $Na_2SiO_3 \cdot 9H_2O$–$CaCl_2$ combination was not selected for subsequent screening because of the intention to avoid chloride introduction. $Na_2SiO_3 \cdot 9H_2O$ was therefore retained as the preferred inorganic component.

The CPAM–HTAB combination (Figure 5d) had an interpolated minimum free swelling rate of approximately 2.769%, higher than the 2.3% measured with HTAB alone. Thus, their combination provided no additional swelling suppression within the tested range.

Overall, the benefits of same-category blending depended on the modifier combination. Although $Na_2SiO_3 \cdot 9H_2O$–$CaCl_2$ achieved the greatest reduction among the inorganic binary systems, chloride avoidance remained an important consideration. Subsequent screening therefore focused on organic–inorganic combinations.

3.1.3. Organic–Inorganic Composite Modification

Figure 6 presents the response surfaces of six organic–inorganic combinations. Most combinations achieved greater swelling suppression than the single-modifier and same-category binary systems, although their effectiveness depended on component type and dosage.

For the $AlCl_3 \cdot 6H_2O$-based combinations (Figure 6a,b), the CPAM and HTAB systems achieved minimum free swelling rates of approximately 0.963% and 0.612%, respectively, both lower than that obtained with $AlCl_3 \cdot 6H_2O$ alone. These results indicate enhanced swelling suppression through organic–inorganic combination.

For the $CaCl_2$-based combinations (Figure 6c,d), the CPAM system achieved a minimum free swelling rate of approximately 2.147%, whereas the HTAB system reached an interpolated minimum of approximately 0.636%. This contrast highlights the strong dependence of swelling suppression on the organic component. Despite the favorable performance of the $CaCl_2$–HTAB system, chloride-containing formulations were not prioritized to avoid introducing chloride ions into the cement-stabilized material.

Among the sodium-silicate-based combinations (Figure 6e,f), $Na_2SiO_3 \cdot 9H_2O$–CPAM achieved a minimum free swelling rate of 0.517%, the lowest among the six organic–inorganic systems, compared with 1.394% for $Na_2SiO_3 \cdot 9H_2O$–HTAB. The CPAM-containing combination also provided greater swelling suppression than the corresponding single-modifier and same-category binary systems. Silicate-based stabilizers can promote interparticle bonding through cementitious product formation and pore filling [19], whereas polyacrylamide treatments can regulate polymer–particle interactions and suppress swelling in expansive materials [23–25]. Their combination may therefore provide complementary benefits, consistent with previous findings on organic–inorganic modification of cement-stabilized pavement materials [28]. However, the individual contributions and interaction mechanisms of the two modifiers cannot be established from the present results.

The $Na_2SiO_3 \cdot 9H_2O$–CPAM system achieved the lowest minimum free swelling rate among the six organic–inorganic combinations (0.517%), representing an 89.7% reduction relative to untreated tuff powder (5.0%). Considering its superior performance over the $Na_2SiO_3 \cdot 9H_2O$–HTAB system (1.394%), dosage–response characteristics, and material applicability, the formulation containing 5.0% $Na_2SiO_3 \cdot 9H_2O$ and 0.5% CPAM was selected for subsequent engineering performance evaluation. This selection represents a swelling-

oriented choice under the tested conditions rather than a global optimization of mechanical and economic performance.

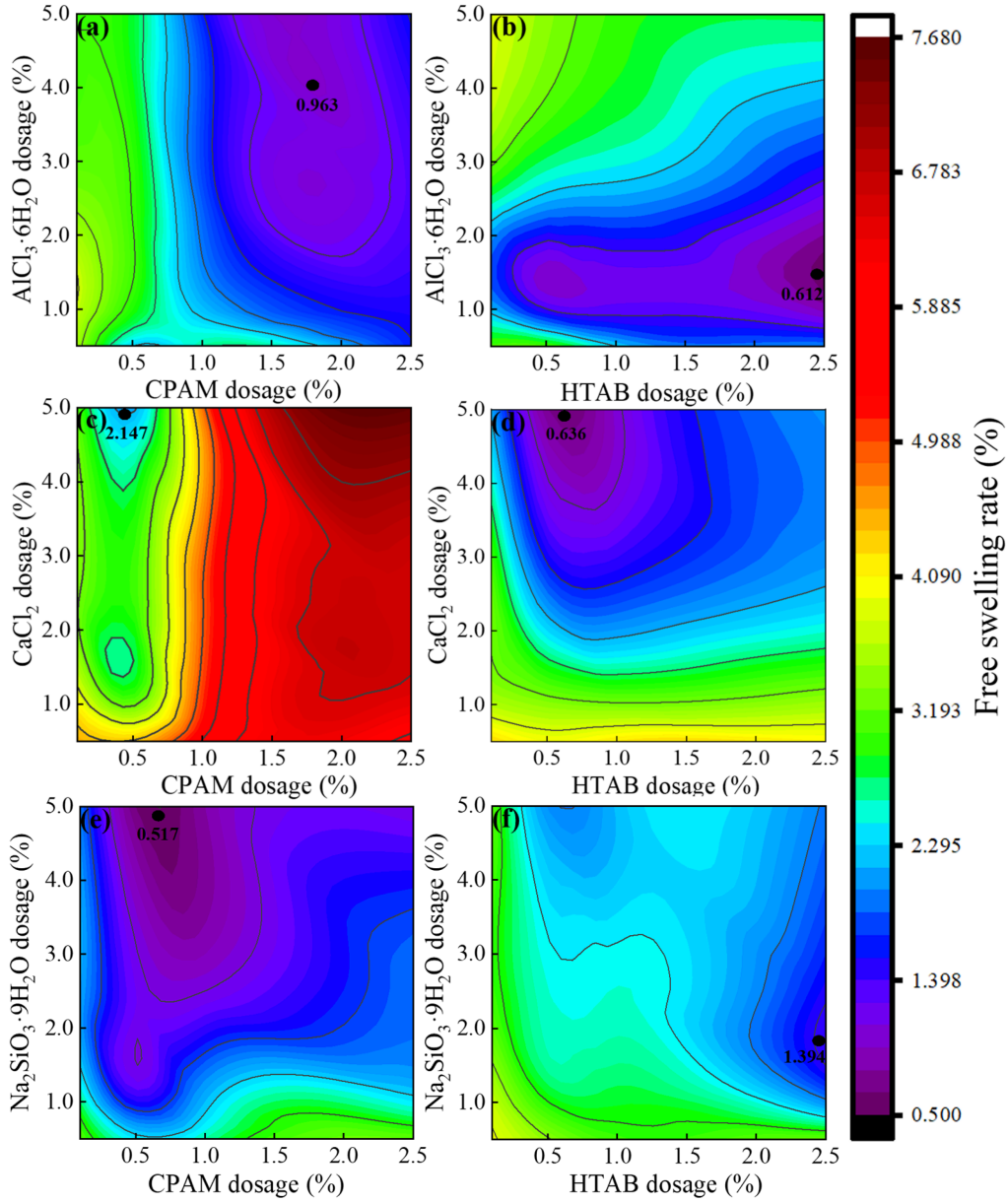

Figure 6. Free swelling rate response contours for organic–inorganic modifier combinations. (**a**,**b**) $AlCl_3·6H_2O$–CPAM/HTAB; (**c**,**d**) $CaCl_2$–CPAM/HTAB; (**e**,**f**) $Na_2SiO_3·9H_2O$–CPAM/HTAB.

3.2. Mechanical Performance

Cement-stabilized tuff without additional modifiers was designated as the control group, while the mixture containing 5.0% $Na_2SiO_3·9H_2O$ and 0.5% CPAM was designated as the modified group. UCS, STS, and compressive resilient modulus were measured at 7, 14, 28, and 90 d to evaluate the effects of composite modification on strength and stiffness development.

3.2.1. UCS

As shown in Figure 7, UCS increased with curing age in both groups, following a two-stage development pattern characterized by relatively rapid growth during 7–28 d and slower growth during 28–90 d. The control group increased from 5.22 MPa at 7 d to 7.56 MPa at 28 d (44.8%), and subsequently reached 8.32 MPa at 90 d. Similarly, the

modified group increased from 5.86 to 8.74 MPa during 7–28 d (49.1%), followed by a further increase to 9.61 MPa at 90 d. This development pattern is consistent with previous findings for cement-stabilized pavement-base materials incorporating tunnel excavation spoil [7].

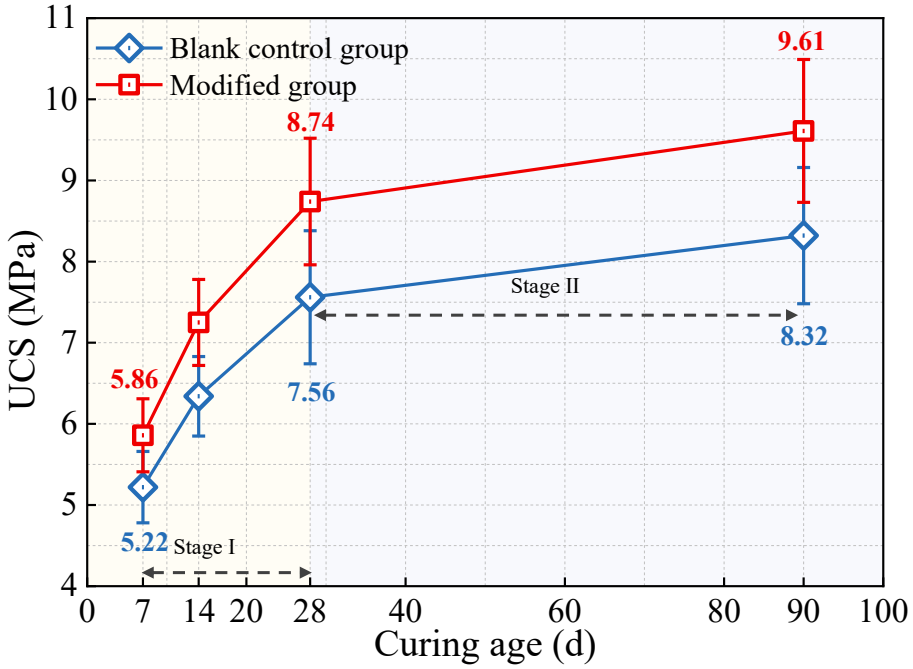

Figure 7. UCS evolution of control and modified groups. Error bars represent ±1 SD (n = 6).

The modified group exhibited higher mean UCS than the control at all curing ages, with relative increases of 12.26%, 15.61%, and 15.50% at 7, 28, and 90 d, respectively. These results indicate a consistent numerical improvement in compressive strength following $Na_2SiO_3 \cdot 9H_2O$–CPAM modification. Previous studies have reported similar strength improvements associated with silicate-based stabilization, CPAM, and organic–inorganic modification [19,25,28]. The observed numerical improvement may be associated with the potential complementary roles of inorganic stabilization and organic interfacial modification, although their individual contributions cannot be distinguished from the present experimental results. Importantly, statistical analysis showed that the between-group difference was significant only at 14 d after Holm adjustment (adjusted $p = 0.046$), whereas no statistically significant differences were identified at 7, 28, or 90 d (adjusted $p > 0.05$).

3.2.2. STS

As shown in Figure 8, STS increased continuously with curing age in both groups, exhibiting a two-stage development pattern. The increase was relatively rapid during 7–28 d but slowed considerably during 28–90 d. Both groups followed a similar overall trend throughout the curing period.

The modified group exhibited higher STS than the control at all curing ages. The relative increases were 18.1%, 27.0%, and 24.3% at 7, 28, and 90 d, respectively. In particular, the 28-d STS increased from 0.89 MPa in the control group to 1.13 MPa in the modified group, representing the greatest relative improvement. Welch's t-test further confirmed that the modified group had significantly higher STS than the control at all curing ages after Holm adjustment (adjusted $p < 0.05$). These findings demonstrate a statistically significant improvement in the splitting tensile performance of cement-stabilized tuff following $Na_2SiO_3 \cdot 9H_2O$–CPAM modification.

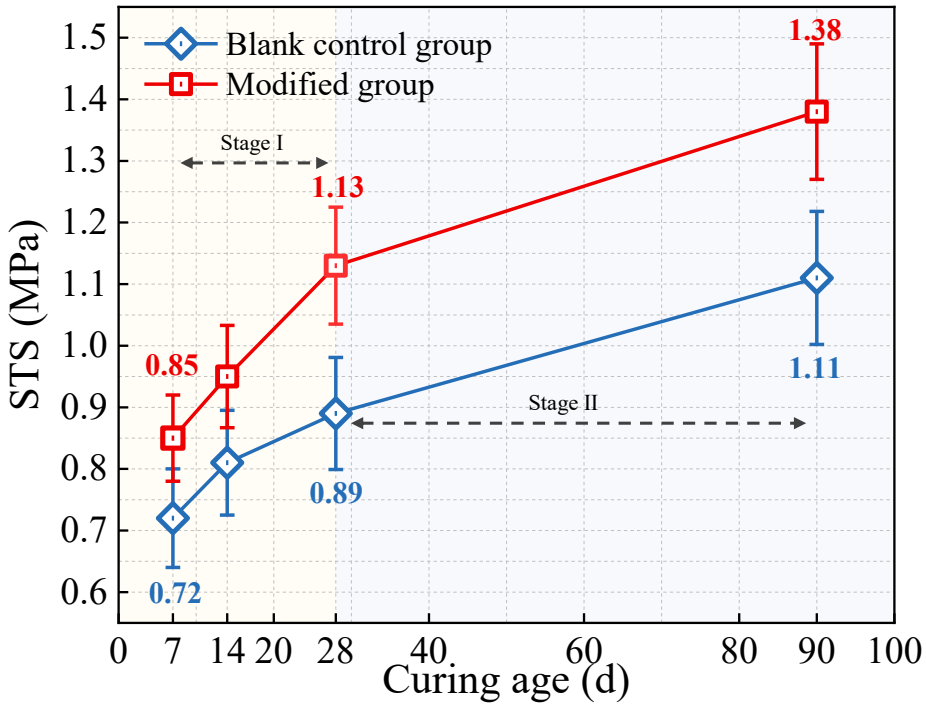

Figure 8. STS evolution of control and modified groups. Error bars represent ±1 SD (n = 6).

At 28 d, the relative increase in STS (27.0%) exceeded that in UCS (15.61%), while the tensile-to-compressive strength ratio increased from 0.118 in the control group to 0.129 in the modified group. These results indicate that the selected composite formulation produced a greater relative improvement in tensile strength than in compressive strength. A similar enhancement in the tensile response of organic–inorganic modified cement-stabilized pavement materials has been reported previously [28].

3.2.3. Compressive Resilient Modulus

As shown in Figure 9, the compressive resilient modulus increased with curing age in both groups, following a two-stage development pattern with faster growth during 7–28 d and slower growth during 28–90 d. The control group increased from 874 MPa at 7 d to 1084 MPa at 28 d (24.0%), before reaching 1147 MPa at 90 d. Correspondingly, the modified group increased from 910 to 1170 MPa during 7–28 d (28.6%) and further reached 1245 MPa at 90 d.

The modified group exhibited higher mean compressive resilient modulus than the control at all curing ages, with relative increases of 4.1%, 7.9%, and 8.5% at 7, 28, and 90 d, respectively. Although the numerical difference generally increased with curing age, none of the between-group differences was statistically significant after Holm adjustment ($p > 0.05$). Therefore, the observed increases indicate a numerical improvement in stiffness rather than a statistically significant enhancement.

Previous studies have shown that the resilient response of crushed tuff is sensitive to moisture conditions, with increasing moisture toward saturation reducing resilient modulus [13], while organic–inorganic modification can improve the modulus response of cement-stabilized pavement materials [28]. In the present study, the modified group maintained a higher compressive resilient modulus than the control following water conditioning. This result indicates that the selected composite formulation contributed to maintaining the stiffness of cement-stabilized tuff under the tested conditions.

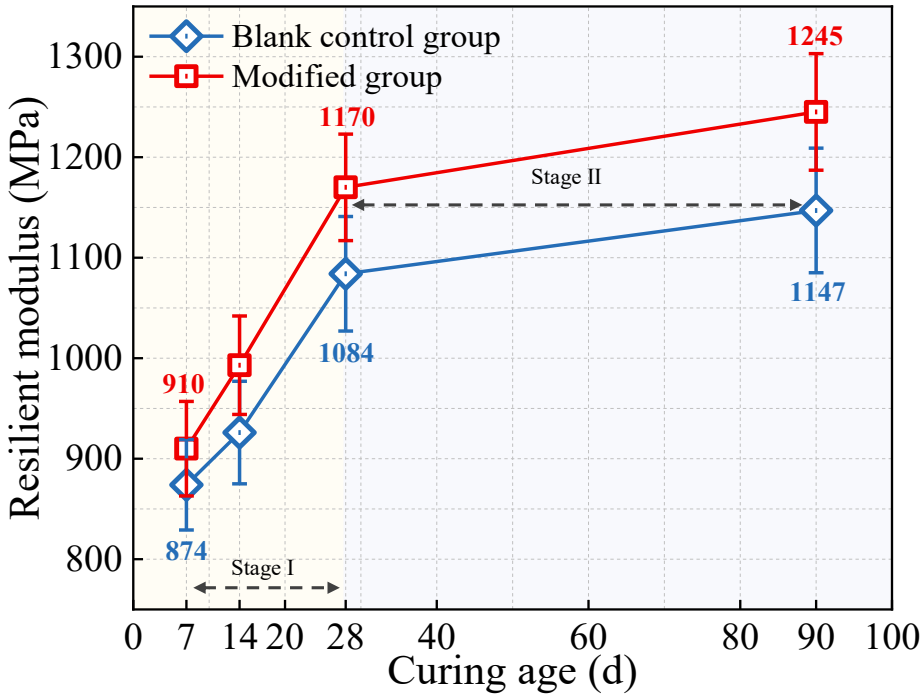

Figure 9. Compressive resilient modulus evolution of the control and modified groups. Error bars represent ±1 SD (n = 6).

Overall, the modified group exhibited higher mean UCS, STS, and compressive resilient modulus than the control at all curing ages. At 28 d, the respective increases were 15.61%, 27.0%, and 7.9%, with the greatest relative improvement observed in STS. Statistical analysis confirmed significant improvements in STS at all curing ages, whereas significant differences in UCS were identified only at 14 d, and no significant differences in compressive resilient modulus were observed. These findings indicate that the most clearly demonstrated mechanical benefit of $Na_2SiO_3 \cdot 9H_2O$–CPAM modification was the enhancement of splitting tensile performance. Although numerical increases were also observed in UCS and compressive resilient modulus, their statistical significance was not consistently established. The individual contributions and interaction effects of the two modifiers cannot be distinguished using the present experimental design.

The greater relative improvement in STS may be associated with the sensitivity of tensile failure to particle bonding and interfacial defects. In contrast, UCS and compressive resilient modulus are also influenced by aggregate interlock and the overall stiffness of the cemented skeleton. This interpretation is consistent with previous findings for organic–inorganic modified cement-stabilized pavement materials [28]. Nevertheless, the specific mechanisms underlying the greater tensile-strength improvement cannot be conclusively established from the present experimental results.

3.3. Shrinkage Behavior

Drying and thermal shrinkage govern the volumetric stability of cement-stabilized semi-rigid pavement bases. Accordingly, the drying and thermal shrinkage responses of the control and modified groups were evaluated to assess the effects of $Na_2SiO_3 \cdot 9H_2O$–CPAM modification.

3.3.1. Drying Shrinkage Behavior

As shown in Figure 10, CDSS exhibited a two-stage development pattern in both groups. During Stage I (0–30 d), shrinkage accumulated rapidly, followed by a markedly slower increase toward a plateau during Stage II (30–90 d). At 30 d, CDSS reached

480 × 10^{-6} and 297.5 × 10^{-6} in the control and modified groups, respectively, approaching their corresponding 90-d values. This indicates that most drying shrinkage occurred during the early drying stage.

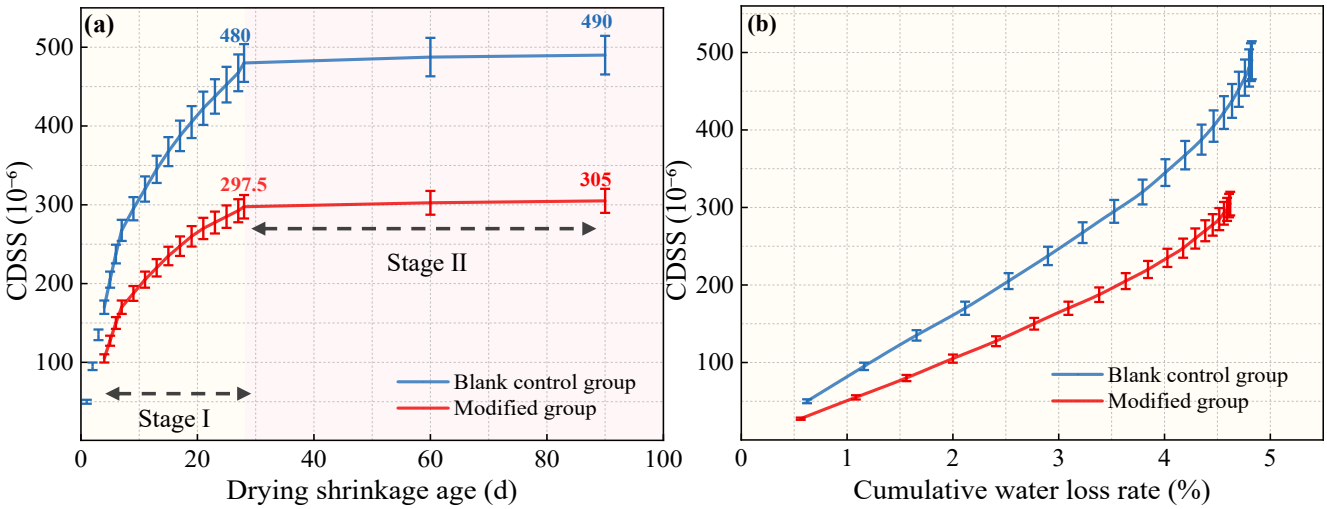

Figure 10. Drying shrinkage properties of control and modified tuff cement-stabilized aggregates. (**a**) CDSS versus drying shrinkage age; (**b**) CDSS versus cumulative water loss rate. Error bars represent ±1 SD.

The modified group consistently exhibited lower CDSS than the control throughout drying (Figure 10a). At 90 d, CDSS decreased from 490 × 10^{-6} to 305 × 10^{-6}, representing a 37.8% reduction. As shown in Figure 10b, both groups exhibited increasing CDSS with cumulative water loss, but the modified group maintained lower shrinkage strain at comparable water-loss levels, indicating reduced moisture-loss-induced deformation.

Previous studies have reported improved volumetric stability of composite-stabilized expansive materials under wetting–drying conditions [21] and reduced drying-induced cracking following polymer modification [23]. Consistent with these findings, the $Na_2SiO_3 \cdot 9H_2O$–CPAM system reduced moisture-loss-induced deformation. Together with the enhanced STS, the lower drying shrinkage suggests a potential improvement in resistance to shrinkage-induced cracking. However, as cracking resistance was not directly evaluated, this interpretation remains inferential and requires verification through dedicated cracking tests.

3.3.2. Thermal Shrinkage Behavior

As shown in Figure 11, both groups exhibited a similar non-monotonic variation in TSC with decreasing temperature. TSC progressively decreased from 40–30 °C to 10–0 °C, reaching a local minimum, before increasing markedly in the 0–−10 °C interval and changing more moderately at lower temperatures. The transition near 0 °C may be associated with pore-water freezing and moisture redistribution. The freezing temperature of pore water depends on pore size, with water in larger pores generally freezing closer to 0 °C, whereas water confined in finer pores may remain unfrozen at lower temperatures [40,41]. The associated ice–water phase transition and ice–pore interactions may further influence the thermal deformation of cementitious materials [41]. The observed response may also reflect the initial moisture condition established during curing (20 ± 2 °C and relative humidity ≥ 97%) and the different thermal deformation characteristics of aggregate particles and cementitious constituents. However, because the moisture content immediately before thermal testing was not independently measured, the contribution of pore-water freezing cannot be quantitatively isolated. Nevertheless, at all curing ages and temperature

intervals, the modified group exhibited lower TSC values than the control, indicating that $Na_2SiO_3 \cdot 9H_2O$–CPAM modification reduced the thermal shrinkage response of cement-stabilized tuff.

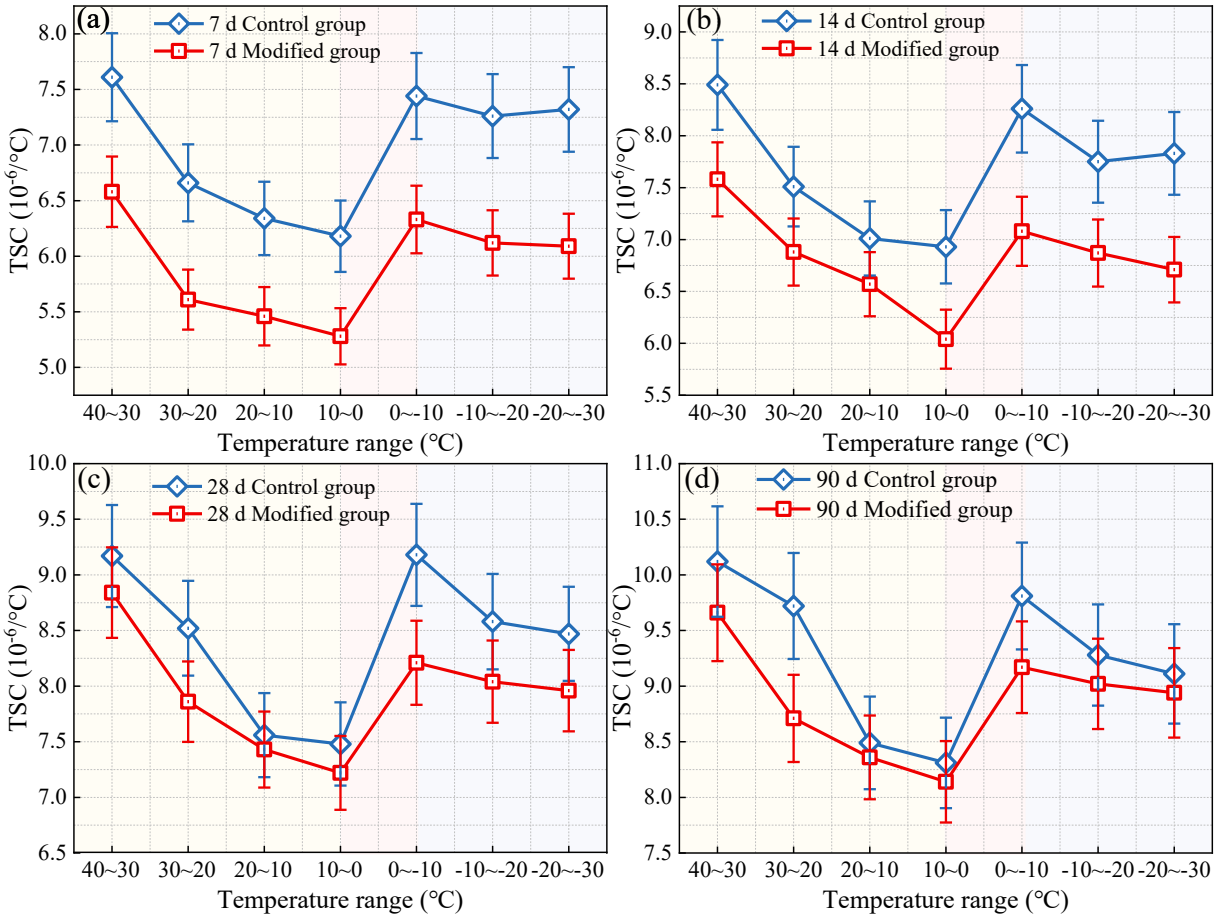

Figure 11. TSC of control and modified groups at different curing ages. (**a**) 7 d; (**b**) 14 d; (**c**) 28 d; (**d**) 90 d. Error bars represent ±1 SD.

As shown in Figure 12, average TSC increased with curing age in both groups but remained consistently lower in the modified group. At 7, 14, 28, and 90 d, the average TSC decreased from 6.97, 7.68, 8.42, and 9.26 $\times$ 10^{-6}/°C in the control group to 5.92, 6.82, 7.93, and 8.86 $\times$ 10^{-6}/°C in the modified group, corresponding to reductions of 15.1%, 11.2%, 5.8%, and 4.3%, respectively. Thus, the modification consistently reduced thermal shrinkage, although its relative effectiveness decreased with curing age.

The decreasing relative effectiveness of the modification with curing age may be related to progressive cement hydration and microstructural development. At early ages, the composite modifiers may exert a stronger influence on moisture migration and interfacial interactions. With continued curing, hydration products develop in both groups, improving particle bonding and altering pore structure and moisture distribution. Previous studies have shown that the thermal deformation of concrete depends on curing age and moisture availability in capillary and gel pores [42]. Consequently, the additional contribution of the composite modifiers to reducing thermal shrinkage may become less pronounced at later ages. This explanation remains tentative because the individual contributions of hydration and moisture redistribution were not independently quantified.

Overall, $Na_2SiO_3 \cdot 9H_2O$–CPAM modification reduced both drying- and thermal-shrinkage deformation, indicating improved volumetric stability of cement-stabilized tuff. Together with the enhanced STS, these improvements suggest a potential benefit

in mitigating shrinkage-induced cracking. However, because cracking resistance was not directly evaluated, this benefit remains inferential and requires verification through restrained shrinkage or direct cracking tests.

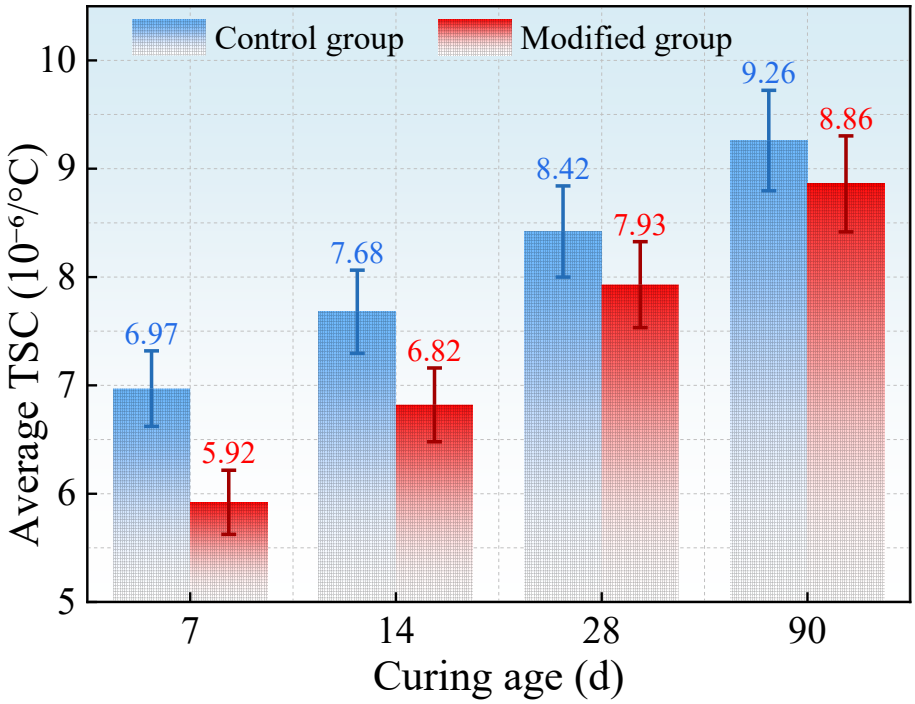

Figure 12. Average TSC of control and modified groups. Error bars represent ±1 SD.

3.4. Microstructural Characterization

The microstructural characteristics of the raw tuff, control, and modified groups were compared using XRD and SEM–EDS to examine the structural features associated with the observed performance changes. Phase composition, particle morphology, and elemental distribution were jointly evaluated to provide complementary evidence for the possible effects of $Na_2SiO_3 \cdot 9H_2O$–CPAM modification.

3.4.1. XRD Phase Analysis

As shown in Figure 13, quartz and albite were the dominant crystalline phases in the raw tuff, control, and modified groups, with their characteristic diffraction peak positions remaining essentially unchanged. This indicates that cement stabilization and $Na_2SiO_3 \cdot 9H_2O$–CPAM modification did not substantially alter the primary crystalline mineral assemblage. Neither quartz nor albite is characterized by pronounced interlayer swelling, suggesting that these dominant phases are unlikely to be the principal sources of the observed swelling behavior. Minor hydrophilic or poorly crystalline constituents may contribute to moisture sensitivity, although their specific identities cannot be established from the available characterization results. No distinct additional crystalline phases were identified after modification, indicating that the observed performance changes were not accompanied by substantial changes in the detectable crystalline phase assemblage.

Relative intensity variations in several quartz and albite reflections were observed in both stabilized groups, particularly in the modified group. However, because diffraction intensity is sensitive to sample preparation and preferred orientation, these variations were not interpreted quantitatively. Hydration products such as calcium silicate hydrate (C–S–H) are typically poorly crystalline or amorphous and may therefore be difficult to identify using conventional XRD. Consequently, the present results cannot independently confirm the formation or quantify the content of specific hydration products. The essentially unchanged

dominant crystalline phases indicate that the observed performance improvements were not accompanied by substantial changes in the detectable crystalline mineral assemblage.

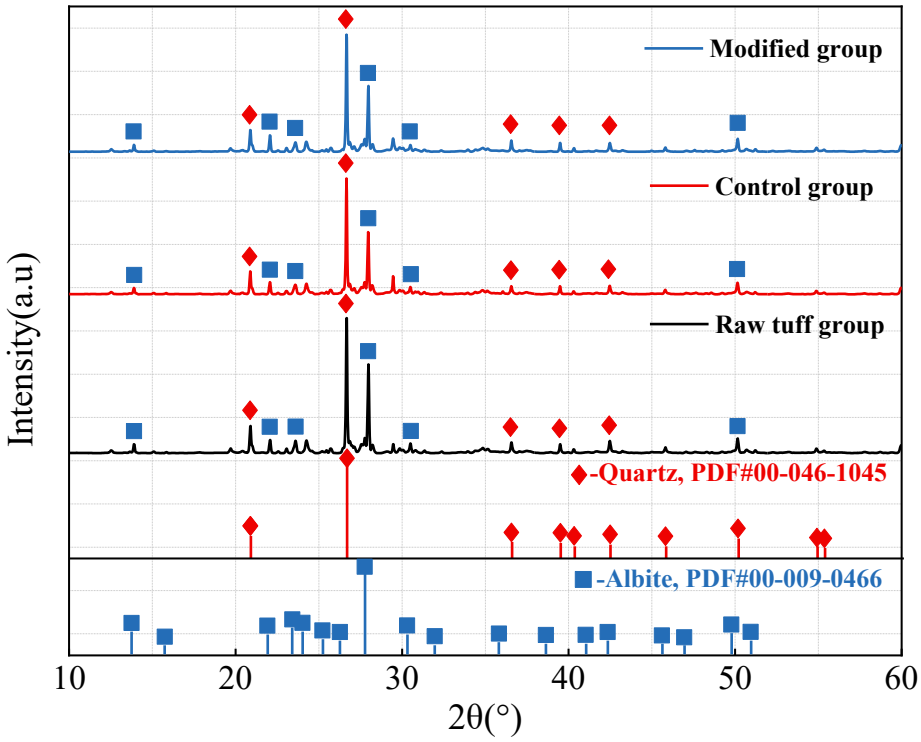

Figure 13. XRD patterns for raw tuff, control, and modified specimens.

Previous studies have reported that sodium-silicate-based stabilization can promote cementitious bonding [19], whereas polymer modification may alter interparticle and interfacial structures without producing distinct new crystalline phases [23]. These findings provide a plausible context for interpreting the observed microstructural differences; however, the specific hydration products and associated chemical reactions cannot be established from the present XRD evidence.

3.4.2. Micromorphology and Elemental Composition Analysis

Figure 14 shows the SEM morphologies of the raw tuff, control, and modified groups at two magnifications. The raw tuff exhibited rough, irregular particle surfaces, visible pores, locally loose structures, and fine lamellar particles attached to larger particles. These heterogeneous and porous features may facilitate water ingress and local deformation, consistent with the moisture sensitivity reported for tuff materials [10–12].

After cement stabilization, the control group (Figure 14c,d) exhibited needle-like and gel-like features that partially filled interparticle voids and connected adjacent particles, producing a denser morphology than that of the raw tuff. These features may be associated with ettringite and C–S–H hydration products, respectively, although their phase identities cannot be confirmed by the present SEM and XRD analyses. Residual macropores and locally discontinuous cemented regions remained visible, indicating persistent structural heterogeneity. Similar pore-filling and particle-bonding features have been reported in silicate-based stabilization systems [19].

In comparison, the modified group (Figure 14e,f) exhibited a more continuous and compact interparticle morphology, with more extensive distributions of gel-like and needle-like features, potentially associated with C–S–H and ettringite, respectively. Fewer visible macropores and tighter interparticle contacts were also observed, suggesting improved pore filling and particle bonding following composite modification. Previous studies have

reported that silicate-based stabilizers promote cementitious structure development [19], whereas polymer modification may improve interfacial characteristics through surface coating and filling [23,25]. These findings provide a plausible interpretation of the observed morphological differences and are consistent with the potential complementary roles of inorganic stabilization and organic interfacial modification. Nevertheless, their individual contributions cannot be distinguished using the present experimental evidence.

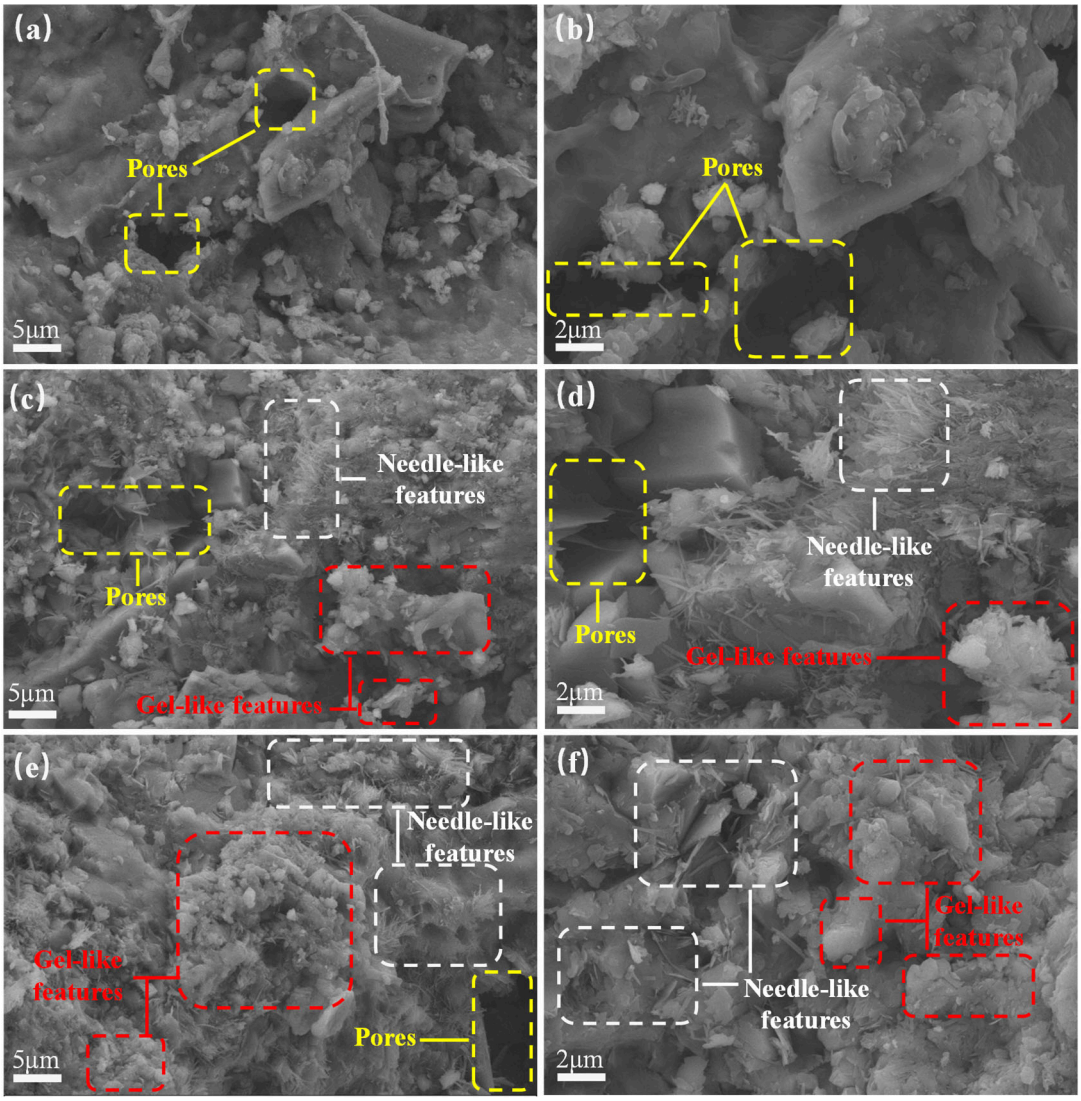

Figure 14. SEM micrographs of the raw tuff, control, and modified groups at two magnifications. (**a**,**b**) Raw tuff group; (**c**,**d**) control group; (**e**,**f**) modified group.

The EDS elemental mass fractions are summarized in Table 4. The raw tuff was dominated by O, Si, and Al, with no detectable Ca in the analyzed region. After cement stabilization, Ca was detected in both the control and modified groups, consistent with the introduction of cement-derived Ca-bearing constituents. Relative to the control group, the modified group exhibited increases in Na (1.34% to 2.59%) and Si (23.51% to 25.95%), consistent with the incorporation of $Na_2SiO_3 \cdot 9H_2O$. Although the Ca content decreased from 5.00% to 3.91%, this difference cannot be used to quantify Ca consumption or secondary hydration because EDS is semi-quantitative and sensitive to sampling location and material heterogeneity. Thus, EDS provides complementary evidence of local elemental composition changes but cannot independently identify or quantify specific hydration products.

Table 4. EDS elemental composition of specimens (wt.%).

Test Sample	O	Na	Mg	Al	Si	K	Ca	Fe
Raw-tuff group	36.58	1.36	–	7.24	29.24	4.21	–	4.45
Control group	37.68	1.34	0.79	7.37	23.51	3.42	5.00	2.79
Modified group	36.53	2.59	–	6.87	25.95	4.03	3.91	2.48

Note: Au originated from the sputter coating and was excluded from the reported compositions. The remaining elemental weight percentages were not renormalized; therefore, their sums are below 100 wt.%.

Overall, the swelling, mechanical, shrinkage, and microstructural results provide complementary evidence of the benefits of $Na_2SiO_3 \cdot 9H_2O$–CPAM modification. The free swelling rate of powdered tuff decreased from 5.0% to 0.517% (an 89.7% reduction), demonstrating improved swelling suppression of the fine tuff fraction. In the full-graded cement-stabilized mixture, the 28-d UCS, STS, and compressive resilient modulus increased by 15.61%, 27.0%, and 7.9%, respectively, while the 90-d cumulative drying shrinkage strain decreased by 37.8%. The thermal shrinkage coefficient also remained lower than that of the control across the tested temperature intervals. These improvements were accompanied by a more compact interparticle morphology, fewer visible macropores, and tighter particle contacts. Although XRD showed no substantial changes in the dominant crystalline phases, EDS revealed local elemental composition differences associated with modifier incorporation. The combined observations suggest that improved particle bonding, pore filling, and interfacial regulation may contribute to the enhanced engineering performance. However, the free swelling results represent the fine tuff fraction rather than the full-graded mixture, and the microstructural evidence is primarily qualitative. Accordingly, these findings provide complementary support for the observed performance improvements rather than definitive evidence of specific chemical mechanisms.

4. Field Implementation and Validation

To assess the applicability of the laboratory-selected $Na_2SiO_3 \cdot 9H_2O$–CPAM stabilization system under practical construction conditions, the modified mixture was implemented in a 267-m full-scale test section of the Mingcun–Dongjiakou Expressway using double-layer continuous paving. This section describes the production, transportation, paving, compaction, and curing procedures and evaluates the constructability, construction quality, and early-age field performance of the modified mixture based on field measurements. The field trial therefore provides a full-scale assessment of the feasibility of translating the laboratory-selected stabilization system into practical pavement-base construction.

4.1. Project Overview

The full-scale test section was located in the third contract section of the Mingcun–Dongjiakou Expressway, Shandong Province, China (Figure 15). The expressway has six lanes, a design speed of 120 km/h, and a 36-cm-thick double-layer cement-stabilized macadam base.

A 267-m section of the left carriageway (K51+920–K52+187) was selected for field validation. The mixture contained 5.0% $Na_2SiO_3 \cdot 9H_2O$, 0.5% CPAM, and 4.5% cement by dry aggregate mass. The 20–30, 10–20, 5–10, and 0–5 mm aggregate fractions accounted for 20%, 36%, 15%, and 29% of the total aggregate mass, respectively. Double-layer continuous paving was adopted throughout the test section.

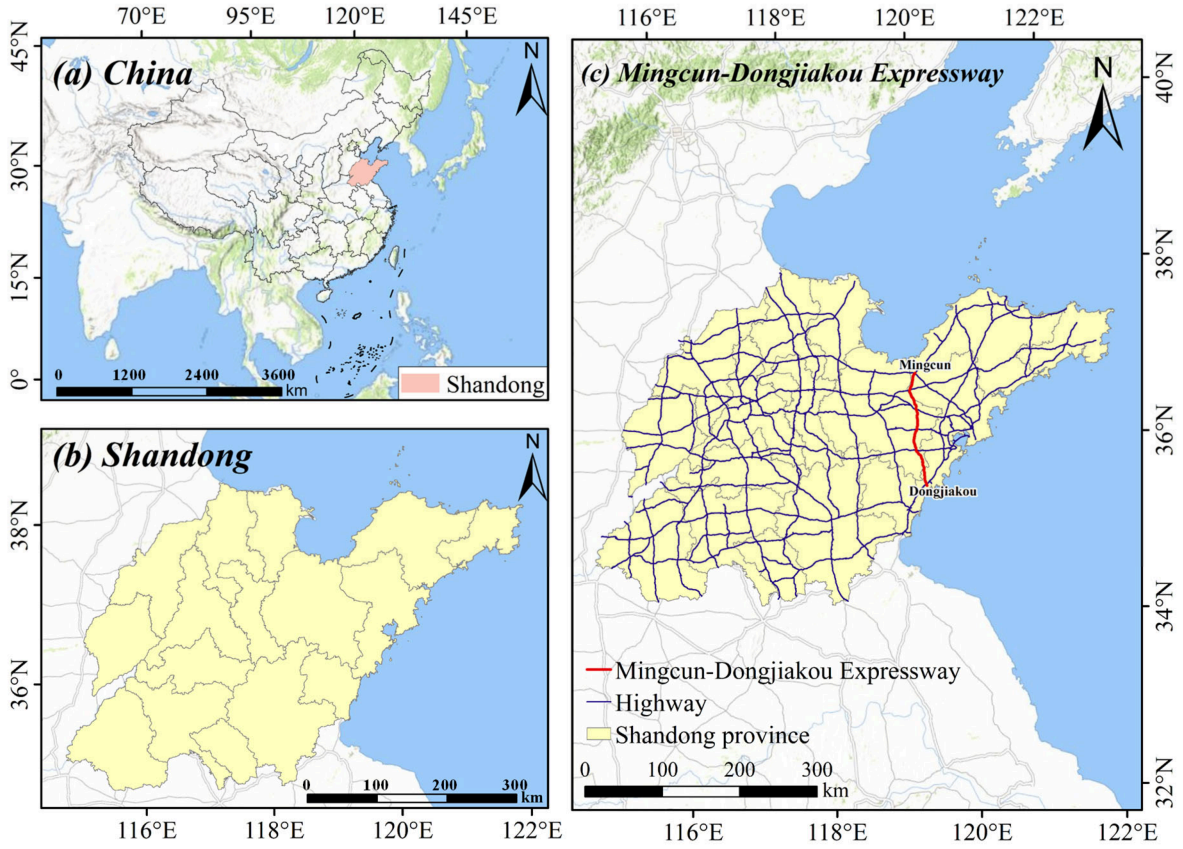

Figure 15. Geographical location map of the Mingcun–Dongjiakou Expressway.

4.2. Key Construction Procedures

The modified mixture was produced in a centralized mixing plant with automatic batching. $Na_2SiO_3 \cdot 9H_2O$ and CPAM were pre-dissolved in the mixing water and added at the prescribed dosages. The mixing time was extended by 10–15 s compared with conventional cement-stabilized macadam to improve modifier dispersion. The water content was adjusted according to ambient conditions, with the discharge moisture content controlled within ±0.5% of the OMC.

Compared with conventional cement-stabilized tuff, the proposed modification system increases additive consumption and initial material costs. However, the modifiers can be incorporated into existing production processes through automatic batching and pre-dissolution, without substantial changes to construction procedures. Its economic feasibility depends on local additive prices and the potential benefits of improved swelling control, mechanical performance, and volumetric stability. A life-cycle cost assessment is required to quantify its overall economic benefits.

The mixture was transported by dump trucks using the three-point loading procedure (Figure 16) to minimize particle segregation. The trucks were covered during transportation to limit moisture loss. Upon arrival, the mixture was inspected for uniformity and moisture condition, and nonconforming material was rejected.

Two pavers operated in echelon to continuously pave the lower and upper base layers (Figure 17). Paving, compaction, and surface treatment of the lower layer, followed by upper-layer paving and compaction, were completed within the initial setting time of the mixture to maintain interlayer continuity while the lower layer remained plastic. Previous studies have reported that double-layer continuous paving improves interlayer bonding and mechanical performance compared with discontinuous construction [32,33], while appropriately timed re-vibration can reduce air voids and improve interlayer structure [34].

Based on the measured initial setting time of approximately 390 min, the construction of both layers was completed within this period.

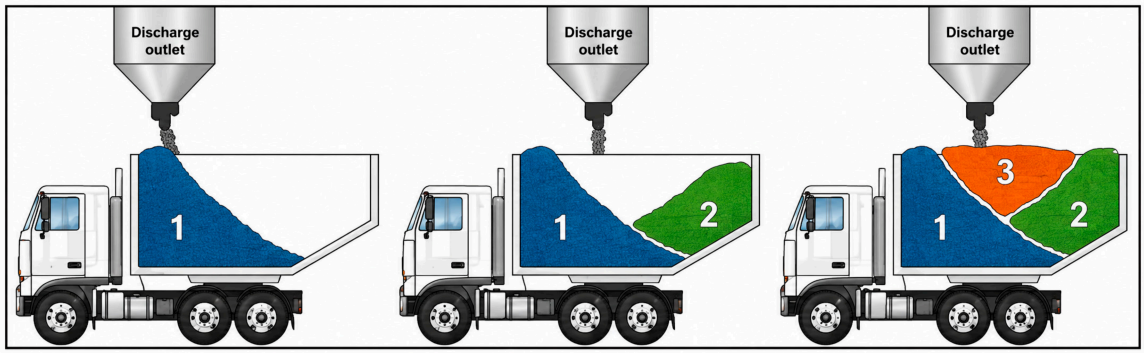

Figure 16. Schematic diagram of the three-point loading method for segregation control of the mixture. (1) First discharge: front of carriage; (2) second discharge: rear of carriage; (3) third discharge: middle of carriage.



Figure 17. Field photograph of base course construction in the test section.

The paving speed was maintained at 1.5–2.0 m/min. Compaction was carried out using steel-drum vibratory and pneumatic-tired rollers, following the sequence of static before vibratory rolling, edges before center, and low before high speed. After initial compaction, the lower-layer surface was roughened before immediate placement and compaction of the upper layer. The completed base was covered with permeable geotextile for at least 7 d of moisture curing, with construction traffic restricted during this period. Transverse butt joints were treated before subsequent paving and compacted to maintain structural continuity and surface regularity.

4.3. Field Construction Quality and Early-Age Performance

Field construction quality was evaluated in accordance with JTG F80/1-2017 [43]. The average compaction degrees of the upper and lower base layers were 98.6% and 98.4%, respectively, both exceeding the specified minimum of 98% for expressway pavement bases. The 7-d core specimens remained intact, without visible fractures or distinct separation at the interface between the two layers, indicating satisfactory compaction and interlayer bonding under the adopted double-layer continuous paving procedure.

The 7-d field UCS measured at seven locations is presented in Figure 18, ranging from 4.9 to 5.5 MPa, with an average of 5.16 MPa. All measurements exceeded the design requirement of 4.5 MPa. Although the average field UCS was lower than the corresponding laboratory value (5.86 MPa), the difference should be interpreted in light of the different testing conditions. Laboratory specimens were immersed in water for 24 h before testing, whereas field cores were extracted directly from the in-situ pavement base. Differences in compaction uniformity, curing conditions, and moisture distribution may also have contributed to the discrepancy. Nevertheless, the relatively narrow range of field UCS values indicates consistent early-age strength across the seven measurement locations.

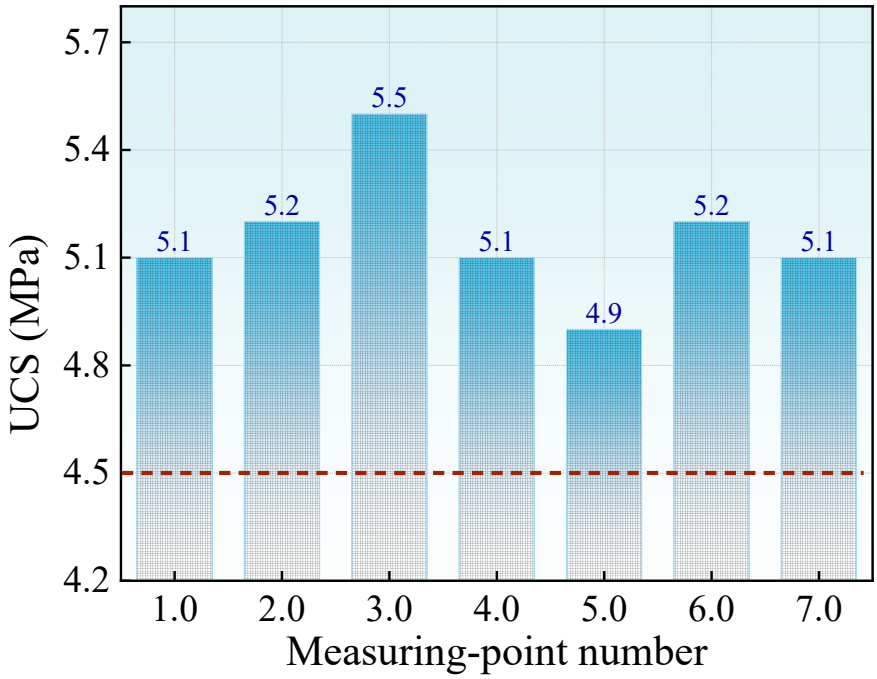

Figure 18. 7-d UCS at different measuring points in the test section.

The measured surface evenness ranged from 4.56 to 6.63 mm, with an acceptance rate exceeding 96%. The top-surface deflection ranged from 8.58 to 12.47 (0.01 mm), indicating a relatively consistent load-bearing response along the test section. Both indicators met the corresponding construction quality-control requirements.

Overall, the field results confirmed that the selected $Na_2SiO_3 \cdot 9H_2O$–CPAM-modified mixture achieved satisfactory construction quality and early-age performance in the 267-m test section, as evidenced by the compaction degree, core integrity, 7-d UCS, surface evenness, and deflection measurements. These findings support the feasibility of applying the laboratory-selected stabilization system in expressway pavement bases and provide field evidence for the resource-efficient utilization of tuff spoil.

The field trial included only the modified mixture, without an unmodified reference section under comparable construction conditions. Therefore, the results demonstrate its constructability and satisfactory early-age performance, but do not allow the specific contribution of the stabilization system to field performance improvement to be quantified. Comparative field trials are needed to further evaluate its effectiveness under practical engineering conditions.

Furthermore, the present field assessment focused on construction quality and early-age performance. The long-term durability of the modified mixture under repeated moisture exposure, freeze–thaw cycles, and cyclic loading remains unverified. Long-term field

monitoring and targeted durability tests are therefore required to evaluate its performance under prolonged service conditions.

5. Conclusions

This study developed a $Na_2SiO_3 \cdot 9H_2O$–CPAM stabilization system for moisture-sensitive expansive tuff spoil and evaluated its performance through laboratory testing, microstructural characterization, and a 267-m full-scale field trial. The main conclusions are as follows:

(1) Organic–inorganic blending effectively enhanced swelling suppression. Within the tested range, the 5.0% $Na_2SiO_3 \cdot 9H_2O$–0.5% CPAM formulation reduced the free swelling rate from 5.0% to 0.517%, an 89.7% reduction, while outperforming the single-modifier and same-category binary systems without introducing chloride ions.

(2) The selected composite formulation yielded higher mean UCS, STS, and compressive resilient modulus than the control, with increases of 15.61%, 27.0%, and 7.9%, respectively, at 28 d. However, statistical significance was confirmed for STS at all tested curing ages and for UCS only at 14 d, whereas the differences in compressive resilient modulus were not statistically significant. The 90-d cumulative drying shrinkage strain decreased by 37.8%, and the thermal shrinkage coefficient remained lower than that of the control across all tested temperature intervals. These results indicate improved mechanical and volumetric performance, although direct cracking resistance was not evaluated.

(3) XRD, SEM, and EDS analyses revealed essentially unchanged dominant crystalline phases, a more compact interparticle morphology, and changes in local elemental composition after composite modification. These observations provide qualitative and semi-quantitative evidence of microstructural changes accompanying the improved engineering performance. However, the specific hydration products and quantitative changes in porosity could not be established from the available characterization results.

(4) The 267-m field trial demonstrated the constructability of the modified mixture using double-layer continuous paving. Within the tested section, compaction degree, 7-d strength, surface evenness, and deflection satisfied the relevant requirements for expressway pavement bases, while core specimens exhibited good integrity and interlayer bonding. However, the absence of an unmodified reference section limits the direct assessment of the modification-related field benefits. Long-term durability under traffic loading and environmental exposure remains to be verified.

Author Contributions: L.M.: Conceptualization, Data Curation, Investigation, Writing—Original Draft, Visualization, Formal Analysis. S.Z.: Supervision, Conceptualization, Methodology, Writing—Review and Editing. J.L.: Supervision, Project Administration, Writing—Review and Editing, Funding Acquisition. H.Z.: Visualization, Validation, Writing—Review and Editing. J.B.: Conceptualization, Supervision, Writing—Review and Editing. All authors have read and agreed to the published version of the manuscript.

Funding: This research was funded by the National Natural Science Foundation of China (52608754; 52478460), the Shandong Natural Science Foundation of China (ZR2024ME054), the Joint Fund of Shandong Natural Science Foundation of China (ZR2025LH142), the Youth Foundation of Shandong Natural Science Foundation of China (ZR2026QC0469; ZR2024QE495), and the Key R&D Program of Shandong Province (2026CXPT181).

Data Availability Statement: The original contributions presented in this study are included in the article. Further inquiries can be directed to the corresponding authors.

Acknowledgments: During the preparation of this work, the authors used ChatGPT (version 5.6 Sol) in order to improve language. After using this tool, the authors reviewed and edited the content as needed and take full responsibility for the content of the published article.

Conflicts of Interest: The authors declare no conflicts of interest.

References

1. Zhuang, S.R.; Liu, Q.; Sun, K.; Lutter, S.; Chen, R.S.; Liu, G. Tracking five decades of global sand and gravel stocks and flows in 184 countries. *Resour. Conserv. Recycl.* **2025**, *222*, 108460. [CrossRef]
2. Zhong, X.Y.; Deetman, S.; Tukker, A.; Behrens, P. Increasing material efficiencies of buildings to address the global sand crisis. *Nat. Sustain.* **2022**, *5*, 389–392. [CrossRef]
3. Cao, Z.; Chu, C.L.; Liu, J.; Su, X.K.; Zhong, X.Y.; Behrens, P. Closing the global sand circularity gap needs a systems approach. *One Earth* **2025**, *8*, 101199. [CrossRef]
4. Chen, Y.H.; Yi, J.Y.; Ren, J.D.; Zhang, H.S.; Pei, Z.S.; Feng, D.C. State of the art of asphalt pavement aggregate and aggregate alternatives in the context of China's long-life pavement concepts. *J. Road Eng.* **2026**, *6*, 91–107. [CrossRef]
5. Duan, X.P.; Wang, Y.M.; Yang, D.W.; Zeng, W.; Du, Y.Q.; Li, N. Evaluation of road performance and carbon emission accounting analysis of recycled aggregates from construction and demolition waste. *Sci. Rep.* **2025**, *15*, 29395. [CrossRef] [PubMed]
6. Dong, H.; Li, H.; Yang, Z.; Shi, H.; Li, L.; Huang, F.; Wang, Z. Feasibility and carbon footprint assessment of tuff tunnel slag powder as a geopolymer precursor. *J. Sustain. Cem.-Based Mater.* **2026**, *15*, 937–949. [CrossRef]
7. Deng, J.S.; Yao, Y.S.; Huang, C. Utilization of tunnel waste slag for cement-stabilized base layers in highway engineering. *Materials* **2024**, *17*, 4525. [CrossRef] [PubMed]
8. García-González, C.; Yepes, J.; Franesqui, M.A. Geomechanical characterization of volcanic aggregates for paving construction applications and correlation with the rock properties. *Transp. Geotech.* **2020**, *24*, 100383. [CrossRef]
9. Wang, X.; Zhang, W.; Zhang, Y.; Qiao, H.; Xue, C.; Mundia, M.M.; An, B. Research on the green preparation of manufactured sand by tuff produced in Gansu China and its influence on the properties of concrete. *Constr. Build. Mater.* **2023**, *409*, 133794. [CrossRef]
10. Zheng, M.Y. Study on the expansion mechanism of tuff in Lancang lead mine. *Chin. J. Rock Mech. Eng.* **2013**, *32*, 216. (In Chinese)
11. Pötzl, C.; Siegesmund, S.; Dohrmann, R.; Koning, J.M.; Wedekind, W. Deterioration of volcanic tuff rocks from Armenia: Constraints on salt crystallization and hydric expansion. *Environ. Earth Sci.* **2018**, *77*, 660. [CrossRef]
12. Chen, X.Z.; Zhang, X.; Li, W.X.; Liu, L.P. Review and prospect of hydro-physical characteristics of tuff and prevention and control technology of tuff tunnel engineering. *Yangtze River* **2023**, *54*, 145–151. (In Chinese) [CrossRef]
13. Cao, Z.G.; Chen, J.Y.; Cai, Y.Q.; Gu, C.; Wang, J. Effects of moisture content on the cyclic behavior of crushed tuff aggregates by large-scale tri-axial test. *Soil Dyn. Earthq. Eng.* **2017**, *95*, 1–8. [CrossRef]
14. Bai, Y.; Chang, S.; Xiao, H.; Li, L.; He, J.; Qiu, J.; Zhou, W.; Deng, Y. Research progress in ecological treatment of expansive soil. *Chin. J. Geotech. Eng.* **2024**, *46*, 60–66, 176. (In Chinese) [CrossRef]
15. Barman, D.; Dash, S.K. Stabilization of expansive soils using chemical additives: A review. *J. Rock Mech. Geotech. Eng.* **2022**, *14*, 1319–1342. [CrossRef]
16. Radhakrishnan, G.; Kumar, A.M.; Raju, P.R.V.G. Laboratory evaluation of the effects of 3-chloride compounds on the geotechnical properties of an expansive subgrade soil. *J. Inst. Eng. India Ser. A* **2017**, *98*, 477–482. [CrossRef]
17. Zhang, L.; Hu, L.M. Physical and chemical properties of bentonite modified by electrochemical treatment. *Int. J. Geomech.* **2024**, *24*, 04024232. [CrossRef]
18. Kodah, R.A.; Rabab'ah, S.R.; Aldeeky, H.H.; Lagaros, N.D.; Abdalla, K.M. Geopolymer stabilization of expansive soils using zeolitic tuff: A sustainable alternative to cement-based stabilization. *Results Eng.* **2025**, *26*, 105386. [CrossRef]
19. Latifi, N.; Vahedifard, F.; Ghazanfari, E.; Horpibulsuk, S.; Marto, A.; Williams, J. Sustainable improvement of clays using low-carbon nontraditional additive. *Int. J. Geomech.* **2018**, *18*, 04017162. [CrossRef]
20. Akula, P.; Naik, S.; Gholami, S.; Kim, Y.R.; Little, D.; Rushing, J. Engineering and mineralogical evaluation of a rapid-strength stabilizer for expansive clays. In *Geo-Congress 2022: Soil Improvement, Geosynthetics, and Innovative Geomaterials*; American Society of Civil Engineers: Reston, VA, USA, 2022; pp. 232–240. [CrossRef]
21. Li, W.; Liu, W.; Wang, B.; Zhan, X.; Zuo, J.; Shan, Y.; Han, S.; Wang, T. Synergistic effects of cement–silica fume composite on expansive soil stabilization: Mechanisms, microstructure, and durability. *Results Eng.* **2025**, *28*, 107811. [CrossRef]
22. Tiwari, N.; Satyam, N.; Puppala, A.J. Strength and durability assessment of expansive soil stabilized with recycled ash and natural fibers. *Transp. Geotech.* **2021**, *29*, 100556. [CrossRef]
23. Yang, F.; Zhao, Y.; Dong, H.; Wang, H.; Niu, W.; Zhao, Z.; Song, F.; Tan, H. Mechanical and microscopic characterization of expansive soils modified by water-soluble polymers. *Sci. Rep.* **2025**, *15*, 2315. [CrossRef] [PubMed]
24. Inyang, H.I.; Bae, S.Y.; Mbamalu, G.W.; Park, S.W. Aqueous polymer effects on volumetric swelling of Na-montmorillonite. *J. Mater. Civ. Eng.* **2007**, *19*, 84–90. [CrossRef]
25. Zhou, S.; Shi, M.; Chen, W.; Zhang, Y.; Wang, W.; Zhang, H.; Li, D. Improved geotechnical behavior of an expansive soil amended with cationic polyacrylamide. *J. Renew. Mater.* **2021**, *9*, 1941–1957. [CrossRef]

26. Erkan, I.; Alp, I.; Çelik, M.S. Characterization of organo-bentonites obtained from different linear-chain quaternary alkylammmonium salts. *Clays Clay Miner.* **2010**, *58*, 792–802. [CrossRef]
27. Hong, Y.Z.; Zeng, L.L.; Zhu, Y.T.; Zhang, C.J.; Zhang, Y. An approach of proportioning multi-source curing agents based on three chemical moduli. *Chin. J. Geotech. Eng.* **2026**, *in press*. (In Chinese) [CrossRef]
28. Gao, Y.; Hao, J.Y.; Li, G.Y.; Lv, X.B.; Wang, W.H.; Wang, K.Y. Study on the performance and mechanism of organic-inorganic synergistic surface modified steel slag cement stabilized macadam. *Constr. Build. Mater.* **2026**, *515*, 145648. [CrossRef]
29. Tanyıldızı, M.; Gökalp, İ. Stabilization of expansive road subgrades with waste paper sludge: Resilient modulus, ANN and modeling approach. *Transp. Geotech.* **2025**, *52*, 101552. [CrossRef]
30. Tavares, A.L.M.; Furlan, A.P.; Fabbri, G.T.P.; Pedreira Junior, J.U. Soil-aggregate-cement mixtures for base pavement layers: A strength and stiffness characterization. *Transp. Geotech.* **2025**, *50*, 101456. [CrossRef]
31. Pham, P.N.; Tran, T.T.T.; Nguyen, P.; Truong, T.A.; Siddique, R.; Liu, Y.; Zhuge, Y. Rubberized cement-stabilized aggregates: Mechanical performance, thermal properties, and effect on temperature fluctuation in road pavements. *Transp. Geotech.* **2023**, *40*, 100982. [CrossRef]
32. Zhang, H.T.; Chen, X.; Wang, Y.B.; Xiong, H.Z. Comparative study on the mechanical properties of base mixture using continuous and discontinuous paving technologies. *Int. J. Pavement Eng.* **2022**, *23*, 3850–3866. [CrossRef]
33. Ding, L.T.; Wang, X.C.; Zhang, M.Y.; Meng, J.Q.; Hu, T. Construction quality control study of double-layer continuous paving for large-thickness cement-stabilized base. *Adv. Civ. Eng.* **2020**, *2020*, 8845642. [CrossRef]
34. Jiang, X.M.; Xu, K.; Li, P.L.; Ma, H.; Sun, C. Effects of re-vibration on mechanical properties and air-void characteristics of cement-stabilised macadam materials. *Road Mater. Pavement Des.* **2024**, *25*, 2604–2622. [CrossRef]
35. Jitsangiam, P.; Nusit, K.; Likitlersuang, S.; Kodikara, J. Using damage evaluation to assess the fatigue behaviour of cement-treated base material from laboratory and full-scale performance tests. *Transp. Geotech.* **2021**, *26*, 100440. [CrossRef]
36. Khan, Z.A.; Balunaini, U.; Costa, S.; Nguyen, N.H.T. A review on sustainable use of recycled construction and demolition waste aggregates in pavement base and subbase layers. *Clean. Mater.* **2024**, *13*, 100266. [CrossRef]
37. *JTG/T F20-2015*; Technical Guidelines for Construction of Highway Roadbases. China Communications Press: Beijing, China, 2015. (In Chinese)
38. *GB/T 50123-2019*; Standard for Geotechnical Testing Method. China Planning Press: Beijing, China, 2019. (In Chinese)
39. *JTG 3441-2024*; Test Methods of Materials Stabilized with Inorganic Binders. China Communications Press: Beijing, China, 2024. (In Chinese)
40. Huo, Y.; Sun, H.; Lu, D.; Chen, Z.; Yang, Y. Mechanical properties of concrete at low and ultra-low temperatures—A review. *J. Infrastruct. Preserv. Resil.* **2022**, *3*, 20. [CrossRef]
41. Xia, J.; Xi, Y.; Jin, W. Temperature-dependent coefficient of thermal expansion of concrete in freezing process. *J. Eng. Mech.* **2017**, *143*, 04017043. [CrossRef]
42. Jeong, J.-H.; Zollinger, D.G.; Lim, J.-S.; Park, J.-Y. Age and moisture effects on thermal expansion of concrete pavement slabs. *J. Mater. Civ. Eng.* **2012**, *24*, 8–15. [CrossRef]
43. *JTG F80/1-2017*; Inspection and Evaluation Quality Standards for Highway Engineering, Section 1: Civil Engineering. China Communications Press: Beijing, China, 2017. (In Chinese)

Disclaimer/Publisher's Note: The statements, opinions and data contained in all publications are solely those of the individual author(s) and contributor(s) and not of MDPI and/or the editor(s). MDPI and/or the editor(s) disclaim responsibility for any injury to people or property resulting from any ideas, methods, instructions or products referred to in the content.